La_3Cl_3BC – Structure, Bonding and Electrical Conductivity

Hui-Yi Zeng[a], Hiroki Okudera[a], Chong Zheng[b], Hansjürgen Mattausch[a], Reinhard K. Kremer[a], and Arndt Simon[a]

[a] Max Planck Institute for Solid State Research, Heisenbergstraße 1, D-70569 Stuttgart, Germany
[b] Department of Chemistry and Biochemistry, Northern Illinois University, DeKalb IL 60115, USA

Reprint requests to Dr. Hansjürgen Mattausch. Fax: 49-711-689-1091.
E-mail: Hj.Mattausch@fkf.mpg.de

Z. Naturforsch. **60b,** 499 – 504 (2005); received February 8, 2005

A new rare earth carbide boride halide, La_3Cl_3BC, has been prepared by heating a mixture of stoichiometric quantities of $LaCl_3$, La, B and C at 1050 °C for 10 days. La_3Cl_3BC (La_3Br_3BC type) crystallizes in the monoclinic system with space group $P2_1/m$ (No. 11), $a = 8.2040(16)$, $b = 3.8824(8)$, $c = 11.328(2)$ Å, $\beta = 100.82(3)^\circ$. In the structure, monocapped trigonal prisms containing B–C units are condensed into chains along the *b* direction, and the chains are further linked by Cl atoms in the *a* and *c* directions. The condensation results in a polymeric anion $^1_\infty$[BC] with a spine of B atoms in a trigonal prismatic coordination by La, and the C atoms attached in a square pyramidal coordination. The B–B and B–C distances are 2.16 and 1.63 Å, respectively. La_3Cl_3BC is metallic. The EH calculation shows that the distribution of valence electrons can be formulated as $(La^{3+})_3(Cl^-)_3(BC)^{5-} \cdot e^-$.

Key words: Rare Earth Boride Carbide Halides, Interstitial Atom, Crystal Structure, Electrical Conductivity, Electronic Structure

Introduction

Metal-rich rare earth (RE) halides with a ratio halogen/metal < 2 exhibit a rich structural chemistry [1 – 3]. Their building units are characteristic metal clusters, mostly filled with interstitial atoms. A variety of elements from throughout the periodic table can be incorporated in the cavities of the building units, RE_6 trigonal antiprisms, RE_6 trigonal prisms and RE_5 square pyramids, as illustrated by numerous examples, such as $ALa_6I_{12}Z$ [4 – 6], La_3X_3Z [7], $Pr_8Cl_7B_7$ [8] and $RE_3X_2BC_2$ [9] (A = alkali metals, X = halides and Z = main group elements).

B–C substructures, such as B–C [9, 10], C–B–C [11, 12], C–B–B–C [9], or C_2–B–B–C_2 [13] entities, have been observed in a few reduced rare earth halides with these atoms as interstitials. In the structure of rare earth boride carbide halides, B atoms always center trigonal RE_6 prisms, and the C atoms of all B–C substructures (B–C distance 1.6 Å) lie near the basis of tetragonal pyramids, while discrete C atoms occur in an RE_6 octahedral environment.

Here we report the preparation, crystal structure, electrical conductivity, as well as the electronic band structure of a new rare earth carbide boride chloride, La_3Cl_3BC.

Experimental Section

Synthesis

Owing to the air and moisture sensitivity of some of the educts and all of the products, all operations were carried out in an argon filled glove box or by standard Schlenk technique.

Lanthanum metal (Alfa Aesar, 99.99%) was filed into fine powder in a drybox (M. Braun). $LaCl_3$ was prepared by the reaction of La_2O_3 with HCl (37%) and NH_4Cl, the product being dried under dynamic vacuum and purified twice by sublimation in a Ta container before use [14]. Graphite (99.4%) was heated at 1000 °C under dynamic high vacuum for 12 hours.

Reaction of a mixture of stoichiometric quantities of La, $LaCl_3$, B, C in sealed Ta tubes at 1050 °C for 10 days, or at 920 °C for 1 day and then at 1100 °C for another 10 days, quantitatively yielded La_3Cl_3BC, according to the X-ray powder diffraction diagram.

Crystallography

Single crystal diffraction

Crystals suitable for single crystal diffraction were sealed in glass capillaries under argon and checked by the Buerger technique. X-ray diffraction intensity data were collected up to $2\theta \sim 60^\circ$ at room temperature on a STOE IPDS II diffrac-

Table 1. Crystal data and structure refinement for La_3Cl_3BC.

Identification code	La_3Cl_3BC
Empirical formula	$BCCl_3La_3$
Formula weight	545.90
Temperature	293(2) K
Wavelength	0.71073 Å
Crystal system	monoclinic
Space group	$P2_1/m$ (No. 11)
Unit cell dimensions	$a = 8.2040(16)$ Å
	$b = 3.8824(8)$ Å; $\beta = 100.82(3)^\circ$
	$c = 11.328(2)$ Å
V	354.40(12) Å^3
Z	2
Density (calculated)	5.116 g/cm^3
Absorption coefficient	18.765 mm^{-1}
$F(000)$	466
Crystal size	$0.19 \times 0.02 \times 0.02$ mm^3
θ Range for data collection	2.53 to 24.98°
Index ranges	$-9 \le h \le 9$,
	$-4 \le k \le 4$,
	$-11 \le l \le 13$
Reflections collected	2313
Independent reflections	728 [R(int) = 0.0623]
Completeness to $\theta = 24.98^\circ$	99.9%
Absorption correction	numerical [15]
Max. and min. transmission	0.2378 and 0.2169
Refinement method	Full-matrix least-squares on F^2 [16]
Data / restraints / parameters	728 / 0 / 44
Goodness-of-fit on F^2	1.058
Final R indices [$I > 2\sigma(I)$]	$R1 = 0.0237$, $wR2 = 0.0606$
R Indices (all data)	$R1 = 0.0263$, $wR2 = 0.0616$
Extinction coefficient	0.0145(9)
Largest diff. peak and hole	1.797 and -1.434 eÅ^{-3}

$R1 = \Sigma||F_o| - |F_c||/\Sigma|F_o|$, $wR2 = (\Sigma(w(F_o^2 - F_c^2)^2)/\Sigma(w(F_o^2)^2))^{1/2}$ and $w = 1/[\sigma^2(F_o^2) + (0.0375P)^2 + 0.2011P]$ where $P = (F_o^2 + 2F_c^2)/3$.

Table 2. Atomic coordinates and equivalent isotropic displacement parameters (Å$^2 \times 10^3$) for La_3Cl_3BC. U_{eq} is defined as one third of the trace of the orthogonalized U_{ij} tensor.

Atom	x	y	z	U_{eq}
La1	0.6109(1)	1/4	0.8091(1)	14(1)
La2	0.2817(1)	3/4	0.5993(1)	12(1)
La3	0.2036(1)	1/4	0.8861(1)	14(1)
Cl1	0.0917(3)	1/4	0.1247(2)	15(1)
Cl2	0.6459(2)	3/4	0.5939(2)	16(1)
Cl3	0.0235(3)	1/4	0.6336(2)	17(2)
C	0.393(1)	3/4	0.8168(9)	22(2)[1]
B	0.529(2)	1/4	0.040(1)	43(3)[1]

$U_{eq} = (1/3)\Sigma_i\Sigma_j U_{ij} a_i^* a_j^* a_i a_j$; [1] refined isotropically.

tometer (Stoe, Darmstadt) with graphite-monochromatized Mo-K$_\alpha$ radiation ($\lambda = 0.71073$ Å). Details on the data collection and structure refinement are summarized in Table 1. The intensities were corrected numerically for absorption [15]. The structure was solved by direct methods and subsequent difference Fourier syntheses, and refined in full-matrix least-squares fitting on F^2 by using the SHELXTL package [16].*

Table 3. Anisotropic displacement parameters (Å$^2 \times 10^3$) for La_3Cl_3BC. The anisotropic displacement factor exponent takes the form: $-2\pi^2[h^2a^{*2}U_{11} + \ldots + 2hka^*b^*U_{12}]$; $U_{23} = U_{12} = 0$.

Atom	U_{11}	U_{22}	U_{33}	U_{13}
La1	13(1)	17(1)	13(1)	−1(1)
La2	14(1)	12(1)	10(1)	2(1)
La3	12(1)	19(1)	9(1)	2(1)
Cl1	16(1)	16(1)	14(1)	1(1)
Cl2	17(1)	19(1)	12(1)	3(1)
Cl3	16(1)	20(1)	14(1)	−1(1)

Table 4. Selected bond lengths [Å] for La_3Cl_3BC.

Bond	Distance	Bond	Distance
La1–C	2.651(6)	La1–B$^{\#2}$	2.82(2)
		La1–B$^{\#3}$	2.96(1)
La2–C	2.46(1)		
		La3–B$^{\#2}$	2.90(2)
La3–C	2.694(7)	La3–B$^{\#3}$	2.93 (1)
La1–Cl1$^{\#3}$	3.098(2)	La1–La3	3.608(1)
La1–Cl2	3.172(2)	La1–La2	3.782(1)
		La1–La1$^{\#1}$	3.8824(8)
La2–Cl3	2.952(2)	La1–La3$^{\#6}$	4.004(1)
La2–Cl2	3.000(2)		
La2–Cl2$^{\#3}$	3.066(2)	La2–La2$^{\#1}$	3.8824(8)
La2–Cl3$^{\#8}$	3.278(2)	La2–La3	3.9389(9)
La3–Cl3	2.963(2)	La3–La3$^{\#1}$	3.8824(8)
La3–Cl1$^{\#2}$	3.013(2)		
La3–Cl1$^{\#8}$	3.089(2)	B–C$^{\#3}$	1.63(2)
		B–B$^{\#11}$	2.16(1)

Symmetry transformations used to generate equivalent atoms: $^{\#1}$ $x,y-1,z$; $^{\#2}$ $x,y,z+1$; $^{\#3}$ $-x+1,-y+1,-z+1$; $^{\#6}$ $-x+1,-y+1,-z+2$; $^{\#8}$ $-x,-y+1,-z+1$; $^{\#11}$ $-x+1,-y,-z$.

X-ray powder diffraction

The X-ray powder diffraction patterns were recorded on a STADI P powder diffractometer (Stoe, Darmstadt), using germanium-monochromatized Mo-K$_\alpha$ radiation ($\lambda = 0.71073$ Å) with the samples enclosed in sealed glass capillaries.

Electrical Conductivity

The electrical conductivity between 5 K and room temperature was measured according to the van der Pauw method [17] on a pressed pellet (6 mm diameter, 1 mm thickness).

Electronic Structure

The density of states (DOS) and the crystal orbital overlap population (COOP) [18] curves were computed us-

*Further details of the crystal structure investigation are available from the Fachinformationszentrum Karls ruhe, D-76344 Eggenstein-Leopoldshafen (Germany), on quoting the depository number CSD-415102, the name of the author(s), and citation of the paper.

ing the tight-binding extended Hückel method (EH) [19]. 435 k-points in the irreducible wedge of the Brillouin zone were employed in the EH computation. The EH parameters for the calculation were (H_{ii} in eV and Slater orbital exponent in parenthesis): C 2s −21.4 (1.625), 2p −11.4 (1.625); B 2s −15.2 (1.3), 2p −8.5 (1.3); Cl 3s −30.0 (2.033), 3p −15.0 (2.033); La 6s −7.67 (2.14), 6p −5.01 (2.08), La 5d −8.21 (3.78 and 1.381, C_1 0.7765, C_2 0.4568).

Results and Discussion

La_3Cl_3BC was initially detected in a reaction of La: $LaCl_3$: B = 5: 1: 3 as a few needle shaped crystals after heating at 950 °C for 10 days, followed by heating at 1000 °C for another 10 days. Structure analysis indicated a crystal composition $La_3Cl_3B_2$ or La_3Cl_3BC. Attempts to prepare pure $La_3Cl_3B_2$ samples were made at different reaction temperatures and durations but failed. EDX analysis on the crystal for which X-ray diffraction data had been collected confirmed the presence of C in different areas of the crystal, however traces of carbon could have been introduced by contamination with vacuum grease which was used for glassware sealing during sample transfer or Ta tube sealing. Preparation of La_3Cl_3BC in quantitative yield was successful by heating the stoichiometric mixture of La, $LaCl_3$, B and C at 1050 °C for 10 days, or at 920 °C for 1 day and then at 1100 °C for another 10 days.

La_3Cl_3BC is isostructural with La_3Br_3BC, Ce_3Cl_3BC and Ce_3Br_3BC [9]. Fig. 1 shows the crystal structure along the *b* direction. The structure consists of $(LaC)_2(La_{6/3}B)_2$ chains which are linked by the Cl atoms along the *a* and *c* directions. The La_6 prisms which are centered by B atoms, are condensed into linear $(La_{6/3}B)_2$ chains by sharing two rectangular prism faces along the *b* direction. Additional La atoms (La2) cap further rectangular faces (La1–La3–La1–La3) on both sides of the $(La_{6/3}B)_2$ chains, resulting in the square pyramidal coordination environment of C atoms. B–C units are formed by the bonding of C atoms to B atoms with a B–C distance of 1.63(2) Å. B–C units are further linked into zigzag B–B chains through apical C atoms by weak B–B contacts (B–B distance: 2.16(1) Å) along [010]. The $(LaC)_2(La_{8/2}B_2)$ chains are linked *via i-a* and *a-i* Cl contacts, according to $(La2C)_2(La1_{4/2}La3_{4/2}B_2)Cl3^{a-i}{}_{2/2}Cl3^{i-a}{}_{2/2}$ $Cl2^{a-i}{}_{2/2}Cl2^{i-a}{}_{2/2}Cl1^{a-i}{}_{2/2}Cl1^{i-a}{}_{2/2}$, in the Schäfer, Schnering notation [20].

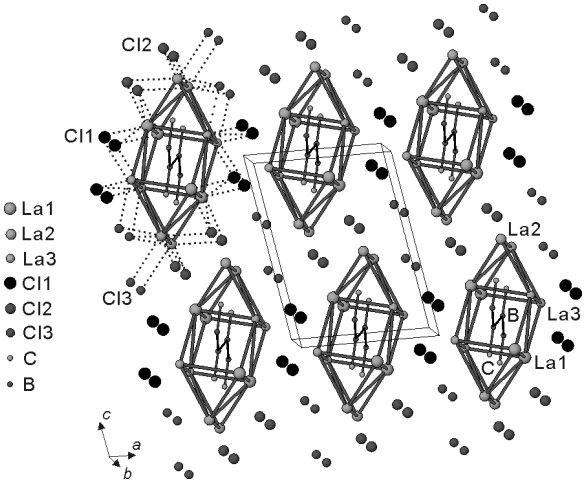

Fig. 1. Projection of the structure of La_3Cl_3BC along [010].

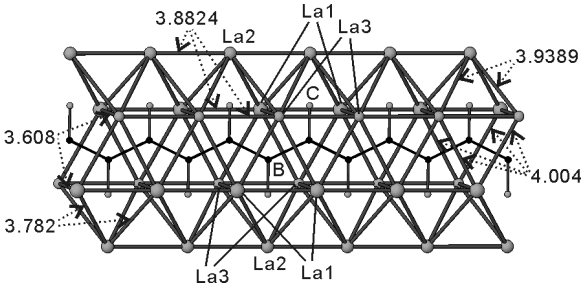

Fig. 2. $(LaC)_2(La_{6/3}B)_2$= La_3BC chain in La_3Cl_3BC.

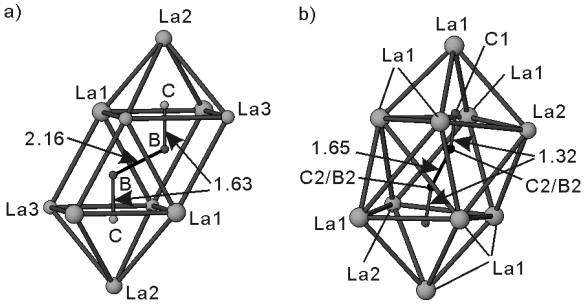

Fig. 3. Comparison of characteristic building units: a) $(LaC)_2La_8B_2$ in La_3Cl_3BC; b) $(LaC)_2[La_4(C/B)]_2$ in $La_5B_2C_6$.

The characteristic building unit $(LaC)_2(La_8B_2)$ in La_3Cl_3BC can be described as a bicapped double trigonal prism embedding a C–B–B–C entity. The $(LaC)_2(La_8B_2)$ unit is similar to the bicapped tetragonal antiprismatic $(LaC)_2[La_4(C/B)]_2$ unit in $La_5B_2C_6$ [21]. In the $(LaC)_2[La_4(C/B)]_2$ unit, two C atoms are located in the square pyramids, while a C/B pair resides in the tetragonal antiprism. How-

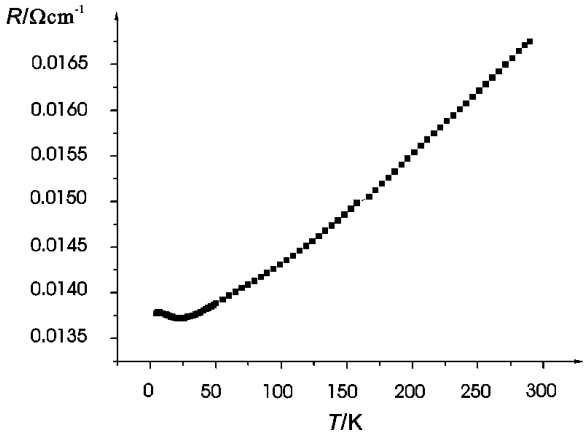

Fig. 4. Temperature dependence of the electrical resistivity of La_3Cl_3BC between 5 and 300 K.

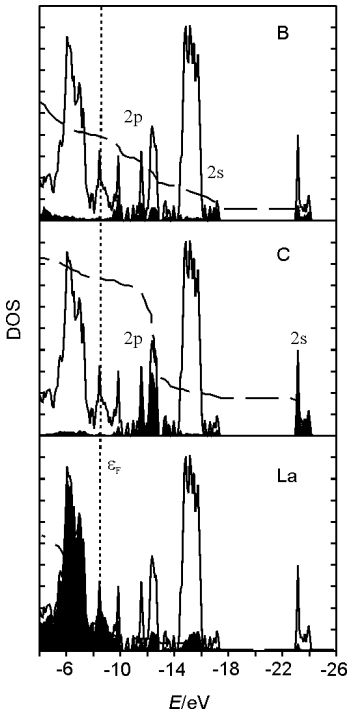

Fig. 5. Calculated EH DOS for La_3Cl_3BC. The solid curves represent the total DOS, the shaded areas and dashed curves correspond to the contribution and integration from the particular atom, respectively, as indicated in each panel. The vertical dotted line indicates the Fermi level.

ever, these building blocks are three-dimensionally connected and due to the antiprismatic surrounding, the C2/B2–C2/B2 distance become as short as 1.65 Å instead of the comparable B–B distance 2.16 Å in La_3Cl_3BC.

The B–C distance of 1.63(2) Å is slightly longer than that in Ce_3Br_3BC (1.57 Å) [4], but much longer than in $La_5B_2C_6$ (1.32 Å) [13]; the B–B separation of 2.16(1) Å is very close to that in Ce_3Br_3BC (2.18 Å) [9]. A Pauling bond order of 0.11 indicates

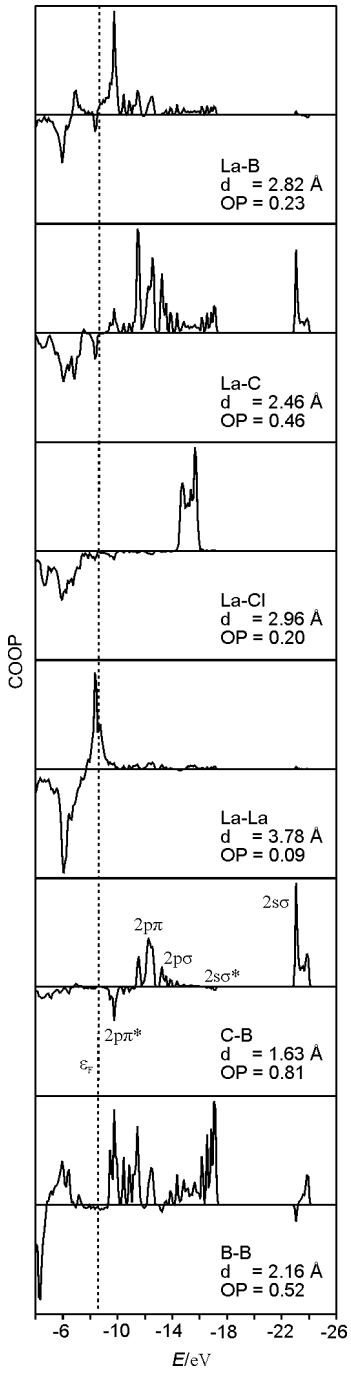

Fig. 6. EH COOP curves of representative bonds in La_3Cl_3BC. The + region is the bonding area and the – region the antibonding area. The bond type, distance and integrated overlap population to the Fermi level are indicated in the inset of each panel. The vertical dotted line is the Fermi level.

weak B–B interactions. The La–La distances are in the expected range of 3.608(1) to 4.004(1) Å, as are the La–Cl distances of 2.952(2) to 3.278(2) Å.

The temperature dependence of the resistivity of La_3Cl_3BC (Fig. 4) indicates that La_3Cl_3BC is a

metal, the resistivity increasing approximately linearly from 25 K to 300 K. In an ionic description, La_3Cl_3BC can be formulated as $(La^{3+})_3(Cl^-)_3(BC)^{6-}$ or $(La^{3+})_3(Cl^-)_3(BC)^{5-} \cdot e^-$, considering the B–B distance to be comparable to that of a normal linkage in borane compounds [22].

The first description corresponds to a hole in the extended $^1_\infty[BC]^{6-}$ chain, whereas the second calls for a delocalized electron in the La framework. Both descriptions predict a metallic behavior of the compound. Of course, this simple view does not refer the extended B–B–B and the strong La–B and La–C interactions in detail. These interactions lead to finite DOS at the Fermi level, a necessary condition for the metallic property as the EH calculation (see the next section) shows.

Both descriptions assume a B–C single bond. Considering charge transfer to the positively charged La framework in the above formulations, the B–C unit should be closer to $(BC)^{5-}$. Fig. 5 shows the calculated DOS using the EH method. The Cl 3s bands, not shown in the figure, lie in the −30 eV region. The peak near −23.5 eV corresponds to C 2s lowered from −21.4 eV of a free C atom, which indicates strong La–C interaction. The Cl 3p bands peak at −15 eV and the C 2p and B 2p bands spread from −14 to −10 eV. The B states are more delocalized due to the weak interactions along the B–B–B zigzag chain at the distance of 2.16(1) Å. A significant La participation below the Fermi level indicates strong covalent La–B and La–C covalent interactions.

Fig. 6 depicts the calculated EH COOP curves of representative bonds in the La_3Cl_3BC structure which all contribute to bonding up to the Fermi level. The C–C and C–B interactions are strong as shown by their corresponding overlap population values, and so are the La–C and La–B contacts. These strong interactions are expected considering their relatively short distances. While the B–B curve is smeared out in a wide energy region due to the B–B–B inter-cell interaction, the C–B interaction is associated with distinct peaks. The assignment of these peaks is $2s\sigma$, $2s\sigma^*$, $2p\sigma$, $2p\pi$ and $2p\pi^*$ with increasing energy, although several peaks are broadened due to the interaction with the extended La framework, making the assignment only semi-quantitative. Nevertheless, these peaks are clearly corresponding to a single C–B bond.

Finally, the question is addressed why the C and not the B atom of the $(BC)^{n-}$ ($n = 5$ or 6) unit is located in the La_5 square pyramid with no interaction between adjacent cells along the *b*-direction. Our EH calculation of a hypothetical $La_3Cl_3C_2$ compound in the La_3Cl_3BC structure has shown that the C atom in the La_5 square pyramid accumulates 0.5 of an electron more than the C atom at the other end. This is likely a consequence of a lower coordination number and/or larger coordination distances within the La framework. The B atom, therefore, should reside at the position which collects less electron density in accordance with the "coloring scheme" [23].

Acknowledgements

The authors thank Mrs. C. Kamella and Mrs. V. Duppel for EDX analysis, and Mrs. G. Siegle for electrical resistance measurement.

[1] G. Meyer, Chem. Rev. **88**, 93 (1988); and references therein.
[2] J. D. Corbett, Dalton Trans. **5**, 575 (1996); and references therein.
[3] A. Simon, Hj. Mattausch, G. J. Miller, W. Bauhofer, R. K. Kremer, in K. A. Gschneidner (Jr), L. Eyring (eds): Handbook on the Physics and Chemistry of Rare Earths, Vol. 15, p. 191, North-Holland, Amsterdam (1991); and references therein.
[4] S. Uma, J. D. Corbett, J. Solid State Chem. **161**, 161 (2001).
[5] E. A. Jensen, J. D. Corbett, Inorg. Chem. **41**, 6199 (2002).
[6] E. A. Jensen, J. D. Corbett, J. Solid State Chem. **172**, 132 (2003).
[7] C. Zheng, O. Oeckler, Hj. Mattausch, A. Simon, Z. Anorg. Allg. Chem. **627**, 2151 (2001).
[8] Hj. Mattausch, O. Oeckler, G. V. Vajenine, R. K. Kremer, A. Simon, Solid State Sci. **1**, 509 (1999).
[9] Hj. Mattausch, O. Oeckler, A. Simon, Inorg. Chim. Acta **289**, 174 (1999).
[10] Hj. Mattausch, A. Simon, Angew. Chem. **107**, 1764 (1995); Angew. Chem. Int. Ed. Engl. **34**, 1633 (1995).
[11] Hj. Mattausch, A. Simon, Angew. Chem. **108**, 1805 (1996); Angew. Chem. Int. Ed. Engl. **35**, 1685 (1996).
[12] O. Oeckler, Hj. Mattausch, A. Simon, Mater. Struct. **5**, 382 (1998).
[13] O. Oeckler, Hj. Mattausch, A. Simon, Z. Anorg. Allg. Chem. **624**, 1834 (1998).
[14] G. Meyer, P. Ax, Mat. Res. Bull. **17**, 1447 (1982).

[15] XSHAPE, Crystal Optimization for Numerical Absorption Correction, Version 1.3, Stoe & Cie GmbH, Darmstadt (1998).
[16] G. M. Sheldrick, SHELXTL Version 5.1, Bruker AXS Inc. (1998).
[17] L. J. Van der Pauw, Philips Res. Rep. **13**, 1 (1995).
[18] S. D. Wijeyesekera, R. Hoffmann, Organometallics **3**, 949 (1984).
[19] M. H. Whangbo, R. Hoffmann, R. B. Woodward, Proc. R. Soc. London **A366**, 23 (1979).
[20] H. Schäfer, H. G. Schnering, Angew. Chem. **76**, 833 (1964); Angew. Chem. Int. Ed. Engl. **3**, 117 (1964).
[21] O. Oeckler, J. Bauer, Hj. Mattausch, A. Simon, Z. Anorg. Allg. Chem. **627**, 779 (2001).
[22] J. J. Briguglio, P. J. Carroll, E. W. Corcoran (Jr.), L. G. Sneddon, Inorg. Chem. **25**, 4618 (1986).
[23] J. K. Burdett, Chemical Bonding in Solids, p. 291, Oxford University Press, New York (1995).